Gadolinite-(Nd), a new member of the gadolinite supergroup from Fe-*REE* deposits of Bastnäs-type, Sweden

Radek Škoda[1,*], Jakub Plášil[2], Renata Čopjaková[1], Milan Novák[1], Erik Jonsson[3,4], Michaela Vašinová Galiová[1,5,6] and Dan Holtstam[7]

[1] Department of Geological Sciences, Faculty of Science, Masaryk University, Kotlářská 2, CZ-611 37 Brno, Czech Republic
[2] Institute of Physics ASCR, v.v.i., Na Slovance 2, Praha 8, CZ-182 21, Czech Republic
[3] Department of Mineral Resources, Geological Survey of Sweden, Box 670, SE-751 28 Uppsala, Sweden
[4] Department of Earth Sciences, Uppsala University, SE-752 36 Uppsala, Sweden
[5] Department of Chemistry, Faculty of Science, Masaryk University, Kotlářská 2, CZ-611 37 Brno, Czech Republic
[6] Central European Institute of Technology (CEITEC), Masaryk University, Kamenice 5, CZ-625 00 Brno, Czech Republic
[7] Swedish Research Council, Box 1035, SE-101 38 Stockholm, Sweden

ABSTRACT

A new member of the gadolinite supergroup, gadolinite-(Nd), IMA2016-013, ideally $Nd_2FeBe_2Si_2O_{10}$, was found in the Malmkärra mine, ~3.5 km WSW of Norberg, south-central Sweden, where it occurs in association with fluorbritholite-(Ce), västmanlandite-(Ce), dollaseite-(Ce), bastnäsite-(Ce) and tremolite. Gadolinite-(Nd) forms anhedral grains up to 150 μm in size, commonly occurring as aggregates of olive green colour. The crystals are transparent with vitreous to adamantine lustre. Gadolinite-(Nd) is brittle with conchoidal fracture, no cleavage or parting was observed. It has a white streak, the Mohs hardness is 6.5–7 and the calculated density is 4.86 g cm^{-3}. Optically, the mineral is weakly pleochroic in shades of olive green, biaxial (–), $n_\alpha = 1.78(1)$, $n_{\beta(calc.)} = 1.80$, $n_\gamma = 1.81(1)$ measured in white light, $2V_{(meas.)} = 62(3)°$. Electron-microprobe and laser ablation inductively coupled plasma mass spectrometry analysis [in wt.%] provided SiO_2 21.77, Y_2O_3 5.49, La_2O_3 2.78, Ce_2O_3 14.04, Pr_2O_3 3.28, Nd_2O_3 19.27, Sm_2O_3 5.30, Eu_2O_3 0.24, Gd_2O_3 4.10, Tb_2O_3 0.36, Dy_2O_3 1.32, Ho_2O_3 0.18, Er_2O_3 0.38, MgO 0.51, CaO 0.14, MnO 0.10, FeO 10.62, B_2O_3 0.10, $BeO_{calc.}$ 8.99, $H_2O_{calc.}$ 0.55 and total 99.52 giving the following empirical formula (based on 2 Si): $(Nd_{0.632} Ce_{0.472}Y_{0.268}Sm_{0.168}Gd_{0.125}Pr_{0.110}La_{0.094}Dy_{0.039}Ca_{0.014}Er_{0.011}Tb_{0.011}Eu_{0.008}Ho_{0.008})_{\Sigma1.957}(Fe_{0.816}Mg_{0.070}Mn_{0.008})_{\Sigma0.894}(Be_{1.984}B_{0.016})_{\Sigma2.000}Si_2O_{9.660}OH_{0.337}$. A weak Raman vibration band at ~3525 cm^{-1} confirms the presence of water in the structure. Gadolinite-(Nd) is monoclinic, $P2_1/c$, with $a = 4.8216(3)$ Å, $b = 7.6985(4)$ Å, $c = 10.1362(6)$ Å, $\beta = 90.234(4)°$, $V = 376.24(6)$ Å^3 and $Z = 2$. The strongest X-ray diffraction lines are [d_{obs} in Å (*hkl*) I_{rel}]: 4.830 (100) 72, 3.603 (021) 37, 3.191 ($\bar{1}$12) 52, 3.097 (013) 35, 2.888 (121) 100, 2.607(113) 49, 2.412 (200) 24. Along with the Malmkärra mine, gadolinite-(Nd) was also recorded also at Johannagruvan and Nya Bastnäs. The minerals of the gadolinite subgroup together with fluorbritholite-(Ce) incorporate the highest fraction of medium-to-heavy rare-earth elements among associated rare-earth element minerals in the Malmkärra mine and possibly in all Bastnäs-type deposits.

*E-mail:rskoda@sci.muni.cz

Introduction

THE mineral gadolinite has a special place in the history of science, and specifically so in chemistry and mineralogy. It was the study of what was then called "ytterbite" from the Ytterby pegmatite north of Stockholm, Sweden, by the Finnish-Swedish chemist Johan Gadolin (1760–1852), that led to the first discovery of a rare-earth element (*REE*) in the form of "yttria" (Gadolin, 1794). Gadolin's yttria was later proven to be a mixture of *REE*s, dominated by yttrium, while the "ytterbite" was finally named gadolinite (Ekeberg, 1802), now gadolinite-(Y). Presently, the *REE*s are very high on the European Union's lists of critical metals (http://europa.eu/rapid/press-release_IP-14-599_en.htm) and neodymium is the most in demand. Systematic research towards the understanding of *REE* ore-forming processes, a better knowledge of the distribution of these metals among the individual ore minerals, and the origin of metals is of increasing interest.

The newly-defined gadolinite supergroup (Bačík *et al.*, 2017) includes silicates, phosphates and arsenates with the general formula $A_2MQT_2O_8\varphi_2$, where the individual structural sites are occupied as follows *A*: Ca, *REE* (Y + lanthanoids) > U, Th, Pb, Mn^{2+} and Bi; *M*: Fe^{2+}, □ (vacancy) > Mg, Mn^{2+}, Zn, Cu, Al; *Q*: Be, B > Li; *T*: Si > P, As, B, Be, S; φ: O, OH > F (Bačík *et al.*, 2017). Based on the *T*-site occupancy, the gadolinite supergroup is divided into the gadolinite $[Si^{4+} > (P^{5+} + As^{5+})]$ and herderite $[(P^{5+} + As^{5+}) > Si^{4+}]$ groups. Moreover, there are two subgroups within the gadolinite group, of which the gadolinite subgroup is dominated by REE^{3+} cations, and the datolite subgroup is dominated by divalent cations, in the *A* site. Accordingly, the *Q*-site is occupied predominantly by Be^{2+} in the gadolinite subgroup and by B^{3+} in the datolite subgroup. The herderite group is also subdivided into the herderite and drugmanite subgroups (cf. Table 1).

Gadolinite-subgroup minerals (particularly gadolinite and hingganite) typically occur in rather metaluminous, fractionated granitic pegmatites with a NYF (Niobium-Yttrium-Fluorine; in the sense of Černý, 1991) signature (e.g. Bjørlykke, 1935; Brotzen, 1959; Haynes, 1965; Vorma *et al.*, 1966; Nilssen, 1973; Bergstøl and Juve, 1988; Smeds, 1990; Kjellman *et al.*, 1999; Pezzotta *et al.*, 1999; Miyawaki *et al.*, 2007; Škoda *et al.*, 2012, 2015; Pieczka *et al.*, 2015), alkaline rocks (e.g. Segalstad and Larsen, 1978; Cámara *et al.*, 2008; Pekov *et al.*, 2007; Lyalina *et al.*, 2014), *REE*-rich

TABLE 1. Minerals of the gadolinite supergroup and their structural formulae (Bačík *et al.*, 2017).

Gadolinite group	
Datolite subgroup	
Datolite	$Ca_2\square B_2Si_2O_8(OH)_2$
Homilite	$Ca_2Fe^{2+}B_2Si_2O_{10}$
Gadolinite subgroup	
Gadolinite-(Ce)	$Ce_2Fe^{2+}Be_2Si_2O_{10}$
Gadolinite-(Nd)	$Nd_2Fe^{2+}Be_2Si_2O_{10}$
Gadolinite-(Y)	$Y_2Fe^{2+}Be_2Si_2O_{10}$
Hingganite-(Ce)	$Ce_2\square Be_2Si_2O_8(OH)_2$
Hingganite-(Y)	$Y_2\square Be_2Si_2O_8(OH)_2$
Hingganite-(Yb)	$Yb_2\square Be_2Si_2O_8(OH)_2$
Minasgeraisite-(Y)	$Y_2CaBe_2Si_2O_{10}$
Herderite group	
Drugmanite subgroup	
Drugmanite	$Pb_2Fe^{3+}\square P_2[O_7(OH)](OH)_2$
Herderite subgroup	
Bergslagite	$Ca_2\square Be_2As_2O_8(OH)_2$
Herderite	$Ca_2\square Be_2P_2O_8F_2$
Hydroxylherderite	$Ca_2\square Be_2P_2O_8(OH)_2$

Alpine-type hydrothermal mineralizations (e.g. Demartin *et al.*, 1993; Bonazzi *et al.*, 2003; Pršek *et al.*, 2010), and some iron-oxide skarn deposits (e.g. Geijer, 1961; Holtstam and Andersson, 2007).

The members of the gadolinite subgroup with a magmatic origin are commonly metamict due to significant amounts of actinides substituting for *REE*, which complicates their structural investigation. Well-crystalline samples are scarce and usually of a hydrothermal origin (Demartin *et al.*, 1993).

A neodymium-dominant analogue of gadolinite-(Y) or gadolinite-(Ce) was suggested by Holtstam and Andersson (2007) from Bastnäs-type skarn deposits (Bergslagen ore province, south-central Sweden), but due to the lack of a sufficient amount of material, they did not provide any data apart from the chemical microanalyses. This paper provides a full characterization, including chemical composition, structural, physical and optical properties of the new mineral gadolinite-(Nd), which was approved recently by the Commission on New Minerals, Nomenclature and Classification (CNMNC) of the International Mineralogical Association (IMA), under the number 2016-013. The name is given in analogy with the other members of the gadolinite subgroup (Bačík *et al.*, 2017), as the neodymium-dominant species. Type material is deposited under catalogue number B 11298 at the Moravian Museum, Brno, Czech Republic.

Geological setting and the type locality

Gadolinite-(Nd) was found in samples from the Malmkärra, Johanna and Nya Bastnäs mines, all belonging to the Fe-*REE* 'Bastnäs-type' skarn deposits in the Bergslagen ore province (Geijer, 1961; Holtstam and Andersson, 2007; Jonsson *et al.*, 2014; Holtstam *et al.*, 2014). The present mineral characterization was only undertaken on material from the Malmkärra mine (60°4′N, 15°51′ E), ~3.5 km WSW of Norberg due to the very small size of gadolinite-(Nd) crystals (<30 μm) at the other localities.

The Bastnäs-type deposits occur in the northwestern part of the Bergslagen ore province, south central Sweden, in the so-called '*REE*-line' (Jonsson and Högdahl, 2013; Goodenough *et al.*, 2016). This is an over 100 km long, north-east-trending, narrow belt within Svecofennian (1.91–1.88 Ga), mainly felsic metavolcanic rocks with discontinuous, interlayered carbonate (marble) horizons. The volcanic sequences were intensively metasomatized at the synvolcanic stage, and much of the carbonates have been replaced by skarn, hosting the localized Fe-*REE* mineralizations. The skarn-hosted Fe-oxide-*REE*-polymetallic mineralization at Bastnäs, in the central part of the *REE*-line, has been dated from the Re-Os contents of molybdenite to give ages between 1.90 and 1.84 Ga. The mineralization is suggested to be the products of reactions between carbonate interlayers with Si, F, Cl, S, CO_2 and *REE*-bearing, high-temperature fluids of a magmatic origin (Holtstam *et al.*, 2014; Sahlström *et al.*, 2015). The term

'Bastnäs-type deposits' was introduced by Geijer (1961) to characterize a group of similar, Fe + *REE* ± Cu ± Mo ± Bi ± Au mineralized skarns that supposedly have a common origin to the Nya Bastnäs deposit. Based mainly on differences in mineral assemblages, Holtstam and Andersson (2007) divided them into two subtypes: deposits of subtype 1 are essentially only enriched in light-rare-earth elements (*LREE*), whereas those of subtype 2 are enriched in both light and heavy-rare-earth elements (*LREE* and *HREE*, respectively).

The Malmkärra deposit (subtype 2) is hosted by a partly dolomitic marble that forms a conformable interlayer within the surrounding, typically extensively altered metavolcanic rocks. The skarn ore body, formed through reactions and replacement of parts of the carbonate interlayer, occurs along the contact with the more extensively altered metavolcanic rocks. Magnetite is the sole ore mineral that was mined, and tremolitic amphibole, humite-group minerals, commonly serpentine-altered, biotite and phlogopite make up the main skarn silicates; sulfide minerals (pyrite, chalcopyrite and molybdenite) are locally present as well (Geijer, 1936). Allanites *sensu lato* represent the most widespread *REE* minerals scattered in the skarn, as well as in the iron ore. During mining, a ~0.5 m thick zone of massive *REE* silicates [dominated by fluorbritholite-(Ce), västmanlandite-(Ce) and dollaseite-(Ce)] was encountered in the deeper levels of the mine, along the contact between the marble and the skarn iron ore (Geijer, 1936; Andersson, 2004). The *REE* minerals reported from the Malmkärra mine are summarized in Table 2.

TABLE 2. List of *REE*-minerals from the Malmkärra mine, after Holtstam and Andersson (2007), Holtstam *et al.* (2005).

Mineral	Formula
Allanite-(Ce)	$(Ce,La)CaFe^{2+}Al_2[Si_2O_7][SiO_4]O(OH)$
Bastnäsite-(Ce)	$(Ce,La)CO_3F$
Cerite-(Ce)	$(Ce,La,Nd)_9(Mg,Fe)Si_7O_{24}(O,OH,F)_7$
Dissakisite-(Ce)	$Ca(Ce,La)MgAl_2[Si_2O_7][SiO_4]O(OH)$
Dollaseite-(Ce)	$Ca(Ce,La)Mg_2Al[Si_2O_7][SiO_4]F(OH)$
Fluorbritholite-(Ce)	$(Ce,Ca)_5[SiO_4]_3F$
Gadolinite-(Ce)	$Ce_2Fe^{2+}Be_2Si_2O_{10}$
Gadolinite-(Nd)	$Nd_2Fe^{2+}Be_2Si_2O_{10}$
Gadolinite-(Y)	$Y_2Fe^{2+}Be_2Si_2O_{10}$
Magnesiorowlandite-(Y)	$(Y,REE)_4MgSi_4O_{14}F_2$
Västmanlandite-(Ce)	$Ca(Ce,La)_3Al_2Mg_2[Si_2O_7][SiO_4]_3F(OH)_2$

The Malmkärra iron mine has a long history. The oldest preserved record is from 1664, with major mining operations taking place from 1885 up to its final closure in 1936 (Geijer and Magnusson, 1944; Andersson, 2004). Malmkärra is also the type locality of västmanlandite-(Ce), see Holtstam *et al.* (2005).

Results

Mineral association, appearance and physical properties

The skarn rock sample ($\sim$10 cm × 10 cm × 5 cm) containing gadolinite-(Nd) was found on the dumps of the Malmkärra mine. Gadolinite-(Nd) forms anhedral grains up to 150 µm in size, occurring as aggregates associated with tremolite, dollaseite-(Ce), västmanlandite-(Ce), fluorbritholite-(Ce) and bastnäsite-(Ce) (Fig. 1). Gadolinite-(Nd) is transparent and, under the optical microscope in thin section, it is pale olive green, while larger fragments are olive green. It has a white streak and a vitreous to adamantine lustre. No visible fluorescence under shortwave or longwave ultraviolet light was observed. The Mohs hardness is between 6.5 and 7. Gadolinite-(Nd) is brittle with a conchoidal fracture; no cleavage or parting was observed. The density (D_{calc}) is 4.86 g cm^{-3}, and was calculated using the empirical formula and unit-cell parameters obtained from the single-crystal X-ray diffraction (XRD) data. A density measurement could not be performed directly due to the lack of suitable material. Optically, gadolinite-(Nd) is weakly pleochroic in shades of olive green, biaxial (–), $n_\alpha = 1.78(1)$, $n_{\beta(calc.)} = 1.80$, $n_\gamma = 1.81(1)$ measured in white light. The poor optical quality of the measured fragments did not allow more precise determination of the refractive indices. The angle of the optical axes, $2V_{(meas.)}$: 62(3)° was
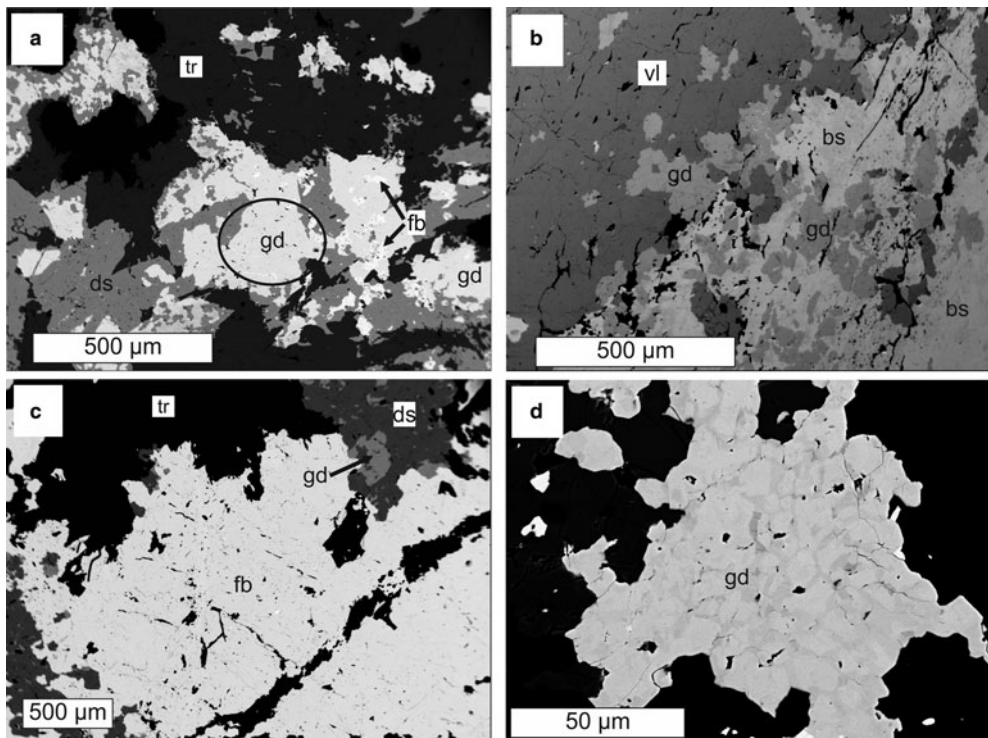
FIG. 1. Back-scattered electron images of gadolinite-(Nd) and associated *REE* minerals from (*a–c*) Malmkärra and (*d*) Johannagruvan. gd-gadolinite-(Nd), ds-dollaseite-(Ce), fb-fluorbritholite-(Ce), tr-tremolite, vl-västmanlandite-(Ce), bs-bastnäsite-(Ce). The aggregate from which the crystals for single-crystal X-ray diffraction and optical study were extracted is indicated by an ellipse. The zoning of the gadolinite-(Nd) from Johannagruvan (*d*) reflects Y-lanthanoids variability; the Y-rich zones are darker.

TABLE 3. Chemical composition of the gadolinite-(Nd) based on the EMP and LA-ICP-MS data.

Constituent	Mean[+]	Range[§]	Det. limit.[ϕ]	Constituent	apfu[+]	Probe standard; X-ray line
SiO_2	21.77	21.59–22.27	0.04	Si	2.000	sanidine, $K\alpha$
Y_2O_3	5.49	3.60–5.83	0.05	Y	0.268	YAG, $L\alpha$
La_2O_3	2.78	2.04–3.08	0.12	La	0.094	$LaPO_4$, $L\alpha$
Ce_2O_3	14.04	11.77–14.3	0.13	Ce	0.472	$CePO_4$, $L\alpha$
Pr_2O_3	3.28	3.12–3.79	0.16	Pr	0.110	$PrPO_4$, $L\beta$
Nd_2O_3	19.27	18.88–22.04	0.17	Nd	0.632	$NdPO_4$, $L\beta$
Sm_2O_3	5.30	5.04–6.08	0.17	Sm	0.168	$SmPO_4$, $L\beta$
Eu_2O_3	0.24	0.16–0.28	0.12	Eu	0.008	$EuPO_4$, $L\beta$
Gd_2O_3	4.10	3.60–4.43	0.18	Gd	0.125	$GdPO_4$, $L\beta$
Tb_2O_3	0.36	0.31–0.43	0.11	Tb	0.011	$TbPO_4$, $L\alpha$
Dy_2O_3	1.32	1.05–1.52	0.12	Dy	0.039	$DyPO_4$, $L\beta$
Ho_2O_3	0.18	0.11–0.21	0.11	Ho	0.005	$HoPO_4$, $L\beta$
Er_2O_3	0.38	0.18–0.38	0.12	Er	0.011	$ErPO_4$, $L\alpha$
MgO	0.51	0.40–0.92	0.04	Mg	0.070	pyrope, $K\alpha$
CaO	0.14	0.14–0.24	0.03	Ca	0.014	wollastonite, $K\alpha$
MnO	0.10	0.10–0.20	0.06	Mn	0.008	spessartine, $K\alpha$
FeO	10.62	10.09–10.93	0.07	Fe	0.816	almandine, $K\alpha$
BeO*	8.99			Be	1.984	
B_2O_3**	0.10	0.06–0.13	0.02	B	0.016	NIST 610
H_2O[$]	0.55			OH	0.337	
Total	99.52			O	9.660	
				ΣREE	1.957	
				M-site vac.	0.106	

[+]Mean of three analyses of the crystal used for structural determination; apfu = atoms per formula unit; *determined from stoichiometry; [§]range of all (11) analyses; **measured by LA-ICP-MS; [ϕ]detection limit in oxides; [$]calculated from charge balance.

measured using extinction by means of a spindle stage and computed by the *EXCALIBR II* software. Dispersion is strong ($r < v$).

Composition

The compositions of gadolinite-(Nd) and associated minerals were determined by means of electron-probe microanalysis (EPMA) with a CAMECA SX100 in wavelength-dispersive mode at an accelerating voltage of 15 kV, a beam current 20 nA and a beam diameter of 5 µm. The standards, X-ray lines and monochromators used for analysis are listed in Table 2. Aluminium, Pb, Tm, Yb and Lu were also analysed for, but their contents were below the detection limit. The peak counting times varied from 10 s for the main elements to 60 s for the minor elements and high and low energy background was counted for ½ of the peak counting time of the relevant analytical line. The raw data were processed using the X-phi matrix correction routine (Merlet, 1994). Based on the counting

statistics, the measurement error expressed as 2σ is approximately <1 rel.% for concentrations of ~20 wt.% and ~8 rel.% for concentrations of ~1=wt.%.

The contents of Be, B and other trace elements below the detection limit of the EPMA were sought for by means of an Agilent 7500ce quadrupole Inductively Coupled Plasma Mass Spectrometer (ICP-MS; Agilent 7500ce, Santa Clara, CA, USA) with an attached UP 213 laser ablation (LA) system (New Wave Research, Inc., Fremont, CA, USA). The LA-ICP-MS system consists of a nanosecond laser Nd:YAG operating at 213 nm (pulse duration of 4.2 ns) and a SuperCell ablation chamber. Ablated material was transported from the sample chamber using helium carrier gas (1 L min^{−1}) and mixed with argon (0.6 L min^{−1}) prior to the torch. Potential polyatomic interferences were minimized by a collision reaction cell in He mode (1 mL min^{−1}). The contents of major to trace elements were determined after laser ablation of individual spots at the following conditions: diameter 55 µm, strength of laser beam 4 J cm^{−2}, frequency 10 Hz and spot

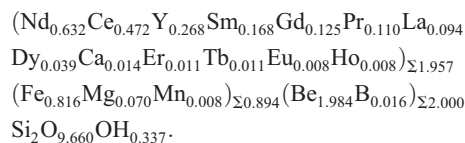TABLE 4. LA-ICP-MS data for gadolinite-(Nd) from Malmkärra (in ppm).

	Mean, $n = 9$	Range	Stand. Dev.
Be	36,400	31,300–39,700	2530
B	301	174–393	61
Y	28,200	21,000–35,900	5500
La	35,000	24,800–43,100	7520
Ce	142,200	123,900–167,600	13,540
Pr	32,500	27,900–39,600	3670
Nd	208,200	176,100–255,700	27,890
Sm	40,200	31,500–54,400	7360
Eu	2050	1560–2770	342
Gd	26,700	21,400–31,900	3410
Tb	2560	1690–3330	508
Dy	8920	5730–13,400	2190
Ho	901	629–1310	204
Er	1730	1180–2340	359
Tm	102	66–162	26
Yb	619	351–10,600	195
Lu	58	32–97	17
Th	3.7	1.8–5.6	1
U	83	45–152	32

ablation time 30 s. The contents of elements of interest were determined using SRM NIST 610 and ^{28}Si for internal calibration and the calculations were performed via peak area of isotopes.

The empirical formula has been calculated on the basis of 2 atoms per formula unit of Si and the amount of OH has been charge balanced to keep the empirical formula electroneutral.

The composition of gadolinite-(Nd) was examined from three thin sections prepared from a single piece of the massive *REE*-silicate-rich sample. The gadolinite shows quite variable chemical composition, particularly in the *REE* pattern and the Y/(*REE*) ratio, but all analyses ($n = 11$) are Nd-dominant and correspond to gadolinite-(Nd), see Table 3. The calcium content is low (0.14–0.24 wt.% CaO). Holtstam and Andersson (2007) performed Mössbauer spectroscopy on the gadolinite-(Ce/Y) from Malmkärra, which revealed the presence of exclusively divalent Fe. Therefore, all Fe is assumed as divalent in gadolinite-(Nd). Apart from Fe, the *M* site is occupied by Mg (0.51–0.66 wt.% MgO) and Mn (0.10–0.14 wt.% MnO). All these cations do not fill the *M* site completely, thus a minor vacancy (0.093–0.143 ☐ pfu) is present. Seven grains, previously analysed by EPMA, were subsequently analysed by LA-ICP-MS to determine the Be and

B content as well as the whole suite of the *REE*s and some trace elements (Table 4). A chondrite-normalized *REE* pattern (using a combination of EPMA and LA-ICP-MS data) shows the maxima at Nd and depletion of the lightest and heavy *REE* as well as a moderate Eu anomaly ($Eu_N*/Eu_N = 0.16$), see Fig. 2. The content of BeO obtained from the LA-ICP-MS analysis ranges from 8.69 to 11.02 wt.% with a mean of 10.11 wt.%. The theoretical BeO content, calculated from stoichiometry, is ~9.0 wt.%. This discrepancy, ~10 rel.%, is still within the analytical error of LA-ICP-MS for Be (~10 rel.%). The average content of B_2O_3 is 0.10 wt.%. Laser ablation ICP-MS also revealed very low U and Th contents in the gadolinite (~80 and ~5 ppm, respectively). Such a low radioactive element content does not affect the crystallinity of the mineral. A small amount of OH (0.34 pfu) resulted from the calculation of an empirical formula. The empirical formula obtained from the mean of three analyses of the crystal used for structural determination is:

$$(Nd_{0.632}Ce_{0.472}Y_{0.268}Sm_{0.168}Gd_{0.125}Pr_{0.110}La_{0.094}$$
$$Dy_{0.039}Ca_{0.014}Er_{0.011}Tb_{0.011}Eu_{0.008}Ho_{0.008})_{\Sigma 1.957}$$
$$(Fe_{0.816}Mg_{0.070}Mn_{0.008})_{\Sigma 0.894}(Be_{1.984}B_{0.016})_{\Sigma 2.000}$$
$$Si_2O_{9.660}OH_{0.337}.$$

The ideal formula is $Nd_2FeBe_2Si_2O_{10}$, which requires 58.16 wt.% Nd_2O_3, 12.42 wt.% FeO, 8.65 wt.% BeO and 20.77 wt.% SiO_2.

A part of the largest grain (150 µm × 100 µm) of gadolinite-(Nd), carefully measured by EPMA, was extracted subsequently from the thin section for the single-crystal X-ray diffraction study. The other parts of this grain were used for determination of the optical properties.

Raman spectroscopy

Raman analysis of gadolinite-(Nd), performed on uncoated polished sections, was undertaken by means of a Horiba LabRAM HR Evolution spectrometer. This dispersive, edge-filter-based system was equipped with an Olympus BX 41 optical microscope, a diffraction grating with 600 grooves per millimetre, and a Peltier-cooled, Si-based charge-coupled device (CCD) detector. Raman spectra of *REE*-bearing minerals are commonly obscured by laser-induced emissions of the *REE* (e.g. Nasdala *et al.*, 2012; Lenz *et al.*, 2015). After careful tests with different lasers (473, 523 and 633 nm), the 633 nm He-Ne laser (10 mW
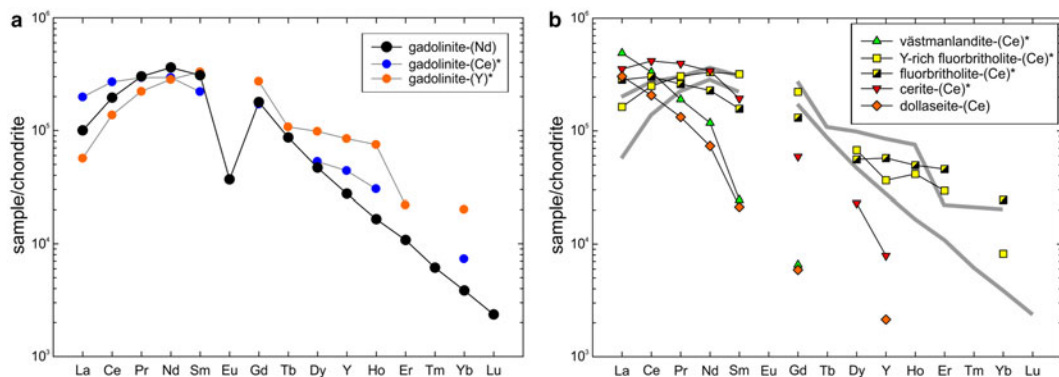
FIG. 2. (*a*) Chondrite-normalized *REE* pattern of gadolinite-(Nd) obtained as a combination of EPMA and LA-ICP-MS data. Patterns of gadolinite-(Ce) and gadolinite-(Y) from Holtstam and Andersson (2007) are plotted for comparison. (*b*) Patterns of other *REE*-silicates from Malmkärra are plotted for visualization of distribution of *REE* among individual structural types. Grey, thick, lines indicate the compositional field of gadolinite-subgroup minerals. Chondrite values of McDonough and Sun (1995) were used for normalization. Data for minerals indicated by an asterisk are taken from Holtstam and Andersson (2007).

at the sample surface) was selected for spectral acquisition to minimize analytical artefacts. With the Olympus 100× objective (numerical aperture 0.9) and the system being operated in the confocal mode, the lateral resolution was ~1 μm. Wavenumber calibration was done using the Rayleigh line and Ne-lamp emissions. The wavenumber accuracy was >0.5 cm^{-1} and the spectral resolution was ~2 cm^{-1}. Band fitting was done after appropriate background correction, assuming combined Lorentzian-Gaussian band shapes using *PeakFit* (Jandel Scientific Software).

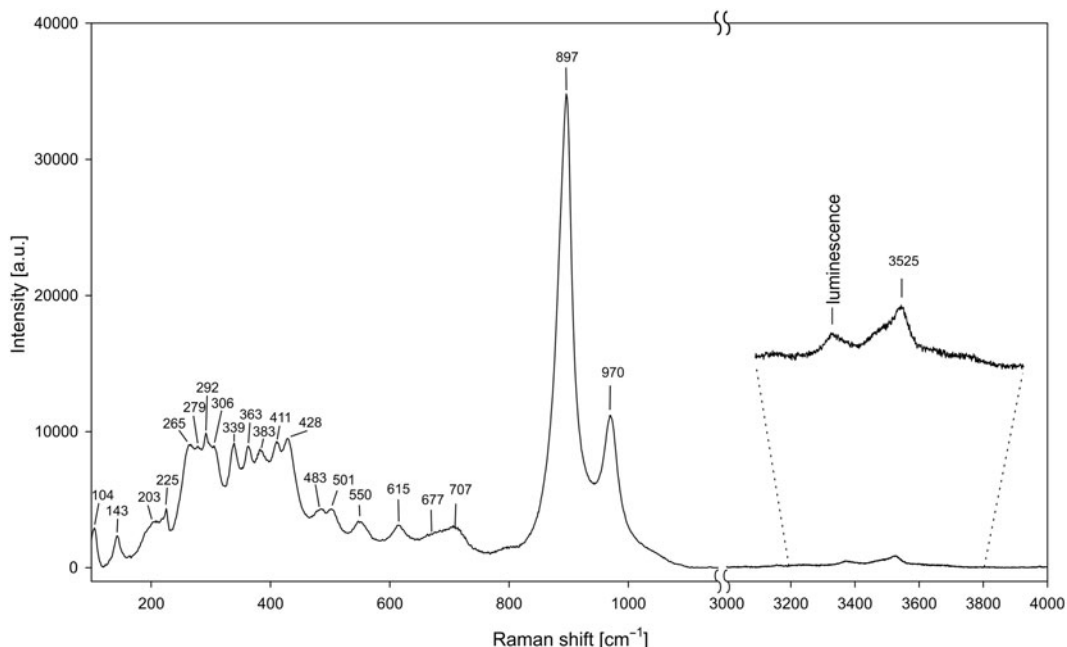The Raman spectrum of gadolinite-(Nd) is shown in Fig. 3. Following the spectroscopic

FIG. 3. Raman spectrum of gadolinite-(Nd) excited by a 633 nm laser.

TABLE 5. Powder XRD data of gadolinite-(Nd) from Malmkärra.

$I_{obs.}$	$d_{obs.}$	$d_{calc.}$	$I_{calc.}$	$h\ k\ l$	$I_{obs.}$	$d_{obs.}$	$d_{calc.}$	$I_{calc.}$	$h\ k\ l$
8	6.147	6.142	32	0 1 1	8	1.805	1.806	13	0 3 4
13	5.085	5.073	20	0 0 2	<5	1.796	1.803	12	0 4 2
72	4.830	4.826	100	1 0 0	6	1.793	1.796	14	0 2 5
18	4.239	4.239	29	0 1 2	<5	1.789	1.791	19	1 4 0
<5	3.843	3.859	2	0 2 0	<5	1.761	1.764	1	$\bar{1}$ 4 1
10	3.798	3.798	11	$\bar{1}$ 1 1			1.764	2	1 4 1
7	3.776	3.792	13	1 1 1	<5	1.756	1.760	<1	2 3 0
37	3.603	3.607	79	0 2 1	<5	1.734	1.735	4	$\bar{2}$ 3 1
13	3.491	3.502	16	$\bar{1}$ 0 2	<5	1.730	1.733	2	2 3 1
		3.492	26	1 0 2	6	1.704	1.707	10	$\bar{2}$ 1 4
52	3.191	3.189	55	$\bar{1}$ 1 2			1.703	13	2 1 4
32	3.179	3.181	48	1 1 2	13	1.690	1.691	16	1 3 4
35	3.097	3.098	55	0 1 3	<5	1.682	1.685	9	$\bar{1}$ 2 5
25	3.014	3.014	25	1 2 0			1.682	8	1 2 5
100	2.888	2.890	73	$\bar{1}$ 2 1	8	1.662	1.664	15	$\bar{2}$ 3 2
		2.888	71	1 2 1			1.662	15	2 3 2
49	2.607	2.610	50	$\bar{1}$ 1 3	5	1.650	1.652	0	0 1 6
		2.604	55	1 1 3	<5	1.604	1.609	7	3 0 0
8	2.534	2.537	4	0 0 4	6	1.596	1.597	11	$\bar{1}$ 0 6
6	2.492	2.493	8	0 3 1	<5	1.593	1.595	11	1 0 6
24	2.412	2.413	31	2 0 0	<5	1.586	1.594	1	$\bar{2}$ 2 4
		2.410	26	0 1 4	<5	1.567	1.564	0	$\bar{1}$ 1 6
16	2.294	2.294	34	0 3 2	<5	1.554	1.557	1	$\bar{3}$ 1 1
<5	2.268	2.270	1	1 3 0			1.556	1	3 1 1
		2.248	3	1 2 3	<5	1.548	1.549	4	0 2 6
11	2.248	2.248	<1	$\bar{1}$ 0 4	<5	1.533	1.535	1	$\bar{3}$ 0 2
		2.247	6	$\bar{2}$ 1 1	<5	1.531	1.532	3	3 0 2
		2.245	1	2 1 1	<5	1.519	1.521	2	2 1 5
6	2.212	2.216	2	$\bar{1}$ 3 1	<5	1.511	1.514	2	$\bar{1}$ 3 5
<5	2.204	2.215	4	1 3 1			1.512	3	1 3 5
10	2.185	2.181	5	$\bar{2}$ 0 2	<5	1.505	1.505	5	$\bar{3}$ 1 2
		2.177	2	2 0 2	<5	1.503	1.503	4	3 1 2
11	2.156	2.158	10	$\bar{1}$ 1 4	5	1.467	1.470	9	$\bar{3}$ 2 1
		2.154	6	1 1 4			1.469	10	3 2 1
6	2.099	2.099	5	$\bar{2}$ 1 2	<5	1.463	1.464	2	$\bar{1}$ 4 4
		2.095	6	2 1 2	<5	1.458	1.463	3	1 4 4
12	2.072	2.073	15	$\bar{1}$ 3 2	5	1.443	1.447	4	$\bar{2}$ 3 4
		2.071	10	1 3 2	10	1.438	1.439	5	2 2 5
6	2.044	2.047	5	0 3 3	<5	1.429	1.429	9	$\bar{3}$ 1 3
		2.046	1	2 2 0	<5	1.365	1.365	0	$\bar{2}$ 1 6
21	2.006	2.006	21	$\bar{2}$ 2 1	<5	1.355	1.357	6	0 2 7
		2.005	24	2 2 1	<5	1.347	1.349	7	$\bar{1}$ 5 3
<5	1.963	1.963	5	0 1 5			1.348	7	1 5 3
<5	1.929	1.929	9	0 4 0	<5	1.341	1.344	1	$\bar{1}$ 4 5
11	1.908	1.906	22	$\bar{2}$ 1 3			1.342	2	1 4 5
18	1.901	1.901	22	2 1 3	<5	1.306	1.307	6	$\bar{1}$ 2 7
		1.896	1	2 2 2			1.305	7	1 2 7
16	1.892	1.895	4	0 4 1			1.236	6	3 4 0
		1.886	3	$\bar{1}$ 3 3	<5	1.233	1.234	2	$\bar{1}$ 6 1
6	1.815	1.820	4	$\bar{1}$ 1 5			1.233	3	1 6 1
		1.816	3	1 1 5	<5	1.227	1.228	4	0 5 5

study of isostructural datolite and herderite (Frost *et al.*, 2013, 2014; Goryainov *et al.*, 2015) the most intense Raman bands at 897 and 970 cm^{-1} are assigned to stretching vibrations of Be–O and Si–O in tetrahedral coordination. The bands in the region 200–750 cm^{-1} are assigned to banding modes of Si–O and Be–O, stretching vibrations of *REE*–O and Fe–O and to lattice vibrations. The weak band at 3525 cm^{-1} is attributed to stretching vibrations of OH units in the gadolinite structure. The local maximum at 3370 cm^{-1} is caused by luminescence as proven by excitation using a 532 nm laser.

X-ray crystallography and structure determination

Powder X-ray diffraction data for gadolinite-(Nd), carefully extracted from the polished section by a diamond microgrinder and powdered under isopropyl alcohol in an agate mortar, were obtained using an Empyrean (PANalytical) powder diffractometer with the solid-state PIXcel^{3D} detector operating in Bragg-Brentano geometry. Data were collected over the range of 5–80°2θ with a step size of 0.013° and counting time of 2 s per step. Positions and intensities of diffraction maxima were obtained from a profile fitting performed with *High-Score3* software (PANalytical). Unit-cell parameters were refined using least-squares based on the positions of 40 reflections utilizing *Celref* software (Laugier and Bochu, 2004). The experimental powder pattern was indexed in accordance with the calculated values of intensities obtained from the single-crystal structure refinement. Powder X-ray diffraction data are given in Table 5. Unit-cell parameters refined from the powder data are $a = 4.826(1)$, $b = 7.717(2)$, $c = 10.147(2)$ Å, $\beta = 90.16°$ and $V = 377.9(2)$ Å^3.

A platy crystal fragment (0.07 mm × 0.06 mm × 0.01 mm) was examined on an Oxford Diffraction Gemini single-crystal diffractometer with Atlas S2 CCD detector, using monochromatized Mo*K*α

TABLE 6. Summary of data collection conditions and refinement parameters for gadolinite-(Nd).

Structural formula	Nd$_{1.942}$FeBe$_{1.931}$Si$_{2.069}$O$_{10}$
Unit-cell parameters	
a, b, c [Å]	4.8216(3), 7.6985(4), 10.1362(6)
ß	90.234(4)
V [Å^3]	376.24(6)
Z	2
Space group	*P*2$_1$/*c*
D_{calc} (g cm^{-3})	5.044
Temperature	301 K
Wavelength	Mo*K*α, 0.7107 Å
Crystal dimensions (mm)	0.069 × 0.059 × 0.019
Collection mode	ω scans to fill an Ewald sphere
Frame width (°), counting time	1.0, 170 s
Limiting θ angles	3.32–28.16°
Limiting Miller indices	$-6 < h < 6$, $-10 < k < 9$, $-13 < l < 12$
No. of reflections	2955
No. of unique reflections	875
No. of observed reflections (criterion)	607 [$I > 3\sigma(I)$]
Absorption correction (mm^{-1}), method	15.483, Gaussian
T_{min}/T_{max}	0.6512/0.8619
R_{int}	0.106
F_{000}	518
Refinement by *Jana2006* on F^2	
Parameters, constraints, restraints	57, 18, 0
R_1, wR_2 (obs)	0.0371, 0.0780
R_1, wR_2 (all)	0.0581, 0.0877
Goof (obs, all)	1.14, 1.05
Weighting scheme, weights	σ, $1/(\sigma^2(F) + 0.0004F^2)$
$\Delta\rho_{min}$, $\Delta\rho_{max}$ (e Å^{-3})	–1.21, 1.56

radiation ($\lambda = 0.71073$ Å) from a conventional sealed X-ray tube and collimated with fibre optics and Mo-Enhance collimator. The unit cell was refined from 1323 reflections using least-squares with the *Crysalis* software (2014, Agilent Technologies, Oxford, UK); ω rotational scans (frame width 1°, counting time 170 s per frame) were adopted to collect a set of three-dimensional intensity data. From a total of 2955 reflections, 875 were independent and 607 classified as observed, with $[I_{obs} > 3\sigma(I)]$. Corrections for background, Lorentz effects and polarization were applied; Gaussian correction for absorption (shape + empirical scaling) was done in *JANA2006* (Petříček *et al.*, 2014) giving a data set with R_{int} of ~10%. Reduction of the data was performed using the *Crysalis* package. The crystal structure of gadolinite-(Nd) was refined from single-crystal data using the structure model for gadolinite-(Y) published in Demartin *et al.* (1993) by full-matrix least-squares using *JANA2006* (Petříček *et al.*, 2014) based on F^2. All non-oxygen atoms were refined with anisotropic displacement parameters. Refinement for 57 parameters and 18 constraints converged to $R = 0.0371$, $wR = 0.0780$ for 607 observed reflections (Goof = 1.14). Details of data collection, crystallographic data and refinement details are given in Table 6. Atom coordinates and displacement parameters are listed in Table 7; selected interatomic distances are provided in Table 8.

The structure refinement of gadolinite-(Nd) provides no significant departure from the published structure results of the isostructural gadolinite-(Y) (Miyawaki *et al.*, 1984; Demartin *et al.*, 1993; Cámara *et al.*, 2008). Minerals of the gadolinite group possess a layer structure composed of two distinct sheets, which are alternating in the **c** direction (Bačík *et al.*, 2014). One sheet is represented by TO_4 and QO_4 tetrahedra and it alternates with a second sheet of AO_8 polyhedra and MO_6 octahedra. In the structure of gadolinite-(Nd), the *T*-site is occupied dominantly by Si^{4+}, the *Q*-site by Be, the *A*-site by Nd^{3+} (and other *REE*) and the *M*-site by Fe^{2+}. During the refinement we treated *A*-sites as only occupied by Nd. We did not model substitutions of a large number of *REE* that have very similar scattering curves for X-rays as we are convinced that such a fit would not make much sense. The refined site occupancies for Nd and Be turned out they be slightly lower than unity (due to the effects of mixing with lighter elements at particular sites). The Mg substitution for Fe, as documented from the wavelength-dispersive spectroscopy analyses, was not successfully confirmed by the structure refinement. The structural formula for gadolinite-

TABLE 7. Atom positions, displacement parameters (equivalent and anisotropic, in Å^2) and bond valences (in valence-units) for gadolinite-(Nd).

Atom	x/a	y/b	z/c	U_{eq}/U_{iso}	U^{11}	U^{22}	U^{33}	U^{12}	U^{13}	U^{23}	Bond valence
Nd	1.00234(13)	0.10860(8)	0.67237(6)	0.0134(2)	0.0158(4)	0.0122(3)	0.0124(4)	−0.0003(3)	0.0054(3)	0.0006(3)	2.88(2)
Fe	1	0.5	0.5	0.0245(9)	0.0224(15)	0.0322(17)	0.0191(15)	0.0012(13)	0.0066(11)	0.0069(12)	1.83(2)
Si1/Be1#	0.5207(6)	0.2252(4)	0.4201(3)	0.0091(10)	0.0113(17)	0.0102(17)	0.0059(16)	−0.0004(13)	0.0035(12)	−0.0012(12)	3.88(4)/ 2.01(2)
Be2/Si2#	0.467(2)	0.4134(15)	0.6613(12)	0.010(4)*	0.015(7)	0.003(6)	0.013(7)	0.003(5)	0.003(5)	−0.001(5)	1.96(4)/ 3.79(7)
O1	0.6835(14)	0.3964(9)	0.3597(7)	0.0092(17)*							2.07(3)
O2	0.7962(15)	0.4120(9)	0.6625(7)	0.0106(17)*							1.72(2)
O3	0.3189(14)	0.1565(9)	0.3014(7)	0.0104(17)*							1.90(3)
O4	0.3272(14)	0.2891(9)	0.5435(7)	0.0079(16)*							2.01(3)
O5	0.7590(14)	0.0913(9)	0.4678(7)	0.0090(16)*							1.92(2)

#refined occupancies for Si1/Be1 are 0.982(17)/0.018(17) and for Be2/Si2 0.947(16)/0.053(16).
*refined with isotropic displacement parameter.

TABLE 8. Selected interatomic distances (in Å) in the structure of gadolinite-(Nd).

Nd–O1[i]	2.448(7)	Fe–O1	2.229(7)
Nd–O2	2.540(7)	Fe–O1[vii]	2.229(7)
Nd–O2[ii]	2.455(7)	Fe–O2	2.037(7)
Nd–O3[iii]	2.576(7)	Fe–O2[vii]	2.037(7)
Nd–O3[iv]	2.701(7)	Fe–O4[v]	2.305(7)
Nd–O4[v]	2.471(7)	Fe–O4[viii]	2.305(7)
Nd–O5	2.382(7)	<Fe–O>	2.190
Nd–O5[vi]	2.392(7)		
<Nd–O>	2.496		
Si1/Be1–O1	1.653(7)	Be2/Si2–O1[viii]	1.646(13)
Si1/Be1–O3	1.633(8)	Be2/Si2–O2	1.589(14)
Si1/Be1–O4	1.639(7)	Be2/Si2–O3[ix]	1.680(14)
Si1/Be1–O5	1.616(7)	Be2/Si2–O4	1.669(13)
<Si1/Be1–O>	1.635	<Be2/Si2–O>	1.646
Si1/Be1– Be2/Si2	2.855(12)		
Si1/Be1–Be2/Si2[viii]	2.903(11)		
Si1/Be1–Be2/Si2[ix]	2.843(12)		

Symmetry codes: (i) x, $-y + 1/2$, $z + 1/2$; (ii) $-x + 2$, $y - 1/2$, $-z + 3/2$; (iii) $-x + 1$, $-y$, $-z + 1$; (iv) $x + 1$, $-y + 1/2$, $z + 1/2$; (v) $x + 1$, y, z; (vi) $-x + 2$, $-y$, $-z + 1$; (vii) $-x + 2$, $-y + 1$, $-z + 1$; (viii) $-x + 1$, $-y + 1$, $-z + 1$; (ix) x, $-y + 1/2$, $z - 1/2$; (x) $-x + 1$, $y + 1/2$, $-z + 1/2$.

(Nd) is therefore $Nd_{1.942}FeBe_{1.931}Si_{2.069}O_{10}$, $Z = 2$. This formula is not electro-neutral due to the fact that the refined occupancies are only a proxy to the real situation, the refinement of all (excluding *REE*) substituting components is beyond the quality of current dataset. However, the refinement of the data suggested that a small amount of Si can enter the *Q*-sites and vice-versa.

Concluding remarks

Rare-earth element ores from the Bastnäs-type deposits are in general characterized by *LREE* enriched and *HREE* depleted patterns (e.g. Holtstam *et al.*, 2014). Taking into consideration the low activity of P and elevated activity of CO_2, the primary *REE* minerals are represented as silicates and carbonates. Among the *REE* phases of the Bastnäs-type mineralization at the Malmkärra mine, the gadolinite-group minerals together with fluorbritholite represent the phases which accommodate the highest amount of middle-rare-earth elements (*MREE*) and *HREE* into their structure. On the other hand, epidote-supergroup minerals, including västmanlandite, are strongly depleted in *MREE* and *HREE* (Fig. 2).

Notably, the new mineral may represent a locally important sink for the critical metal neodymium in deposits of the Bastnäs-type. Geijer (1936) reported törnebohmite as occurring locally in "not insignificant amounts" at Malmkärra, while Holtstam and Andersson (2007) make no mention of having observed this mineral. Considering their, in part similar, optical properties, it seems possible that Geijer's törnebohmite could represent (a misidentified) gadolinite. Additionally, new observations also suggest that it may be more abundant than hitherto known in other Bastnäs-type mineralizations, specifically in the Johanna and Nya Bastnäs mines.

Acknowledgements

References

Andersson, U.B. (2004) The Bastnäs-type REE-mineralisations in north-western Bergslagen, Sweden. *Sveriges Geologiska Undersökning Rapporter and Meddelanden*, **119**, 34.

Bačík, P., Fridrichová, J., Uher, P., Pršek, J. and Ondrejka, M. (2014) The crystal chemistry of gadolinite-datolite group silicates. *The Canadian Mineralogist*, **52**, 625–642.

Bačík, P., Miyawaki, R., Atencio, D., Cámara, F. and Fridrichová, J. (2017) Nomenclature of the Gadolinite Supergroup. *European Journal of Mineralogy*, **29**, 1–16.

Bergstøl, S. and Juve, G. (1988) Scandian ixiolite, pyrochlore and bazzite in granite pegmatite in Tørdal, Telemark, Norway. A contribution to the mineralogy and geochemistry of scandium and tin. *Mineralogy and Petrology*, **38**(4), 229–243.

Bjørlykke, H. (1935) The mineral paragenesis and classification of the granite pegmatites of Iveland, Setesdal, South Norway. *Norsk Geologisk Tidsskrift* **14**, 211–311.

Bonazzi, P., Bindi, L. and Parodi, G. (2003) Gatelite-(Ce), a new *REE*-bearing mineral from Trimouns, French Pyrenees: Crystal structure and polysomatic relationships with epidote and törnebohmite-(Ce). *American Mineralogist*, **88**, 223–228.

Brotzen, O. (1959). Mineral-Association in Granitic Pegmatites: A Statistical Study. *Geologiska Föreningen i Stockholm Förhandlingar*, **81**, 231–296.

Cámara, F., Oberti, R., Ottolini, L., Della Ventura, G. and Bellatreccia, F. (2008) The crystal chemistry of Li in gadolinite. *American Mineralogist*, **93**, 996–1004.

Černý, P. (1991) Rare-element granitic pegmatites, Part 1: anatomy and internal evolution of pegmatite deposits. *Geoscience Canada*, **18**, 49–67.

Demartin, F., Pilati, T., Diella, V., Gentile, P. and Gramaccioli, C.M. (1993) A crystal–chemical investigation of alpine gadolinite. *The Canadian Mineralogist*, **30**, 127–136.

Ekeberg, A.G. (1802) Upplysning om ytterjordens egenskaper, i synnerhet i jämförelse med Berylljorden: om de fossilier, hvari förstnämnde jord innehålles, samt om en ny upptäckt kropp af metallisk natur. *Kongliga Vetenskaps Academiens Nya Handlingar*, **23**, 68–83.

Frost, R.L., Xi, Y., Scholz, R., Lima, R.M.F., Horta, L.F.C. and Lopez, A. (2013) Thermal analysis and vibrational spectroscopic characterization of the boro silicate mineral datolite–CaBSiO$_4$(OH). *Spectrochimica Acta Part A: Molecular and Biomolecular Spectroscopy*, **115**, 376–381.

Frost, R.L., Scholz, R., López, A., Xi, Y., de Siqueira Queiroz, C., Belotti, F.M. and Cândido Filho, M. (2014) Raman, infrared and near-infrared spectroscopic characterization of the herderite–hydroxylherderite mineral series. *Spectrochimica Acta Part A: Molecular and Biomolecular Spectroscopy*, **118**, 430–437.

Gadolin, J. (1794) Undersökning af en svart tung stenart ifrån Ytterby stenbrott i Roslagen. *Kongliga Vetenskaps Academiens Nya Handlingar*, **15**, 137–155.

Geijer, P. (1936) Norbergs berggrund och malmfyndigheter. *Sveriges Geologiska Undersökning*, **Ca 24**, 162 pp.

Geijer, P. (1961) The geological significance of the cerium mineral occurrences of the Bastnäs type in central Sweden. *Arkiv för mineralogi och geologi*, **3**, 99–105.

Geijer, P. and Magnusson, N. H. (1944) De mellansvenska järnmalmernas geologi. *Sveriges Geologiska Undersökning*, **Ca 35**, 654 pp.

Goodenough, K.M., Schilling, J., Jonsson, E., Kalvig, P., Charles, N., Tuduri, J., Deady, E.A., Sadeghi, M., Schiellerup, H., Müller, A., Bertrand, G., Arvanitidis, N., Eliopolous, D.G., Shaw, R.A., Thrane, K. and Keulen, N. (2016) Europe's rare earth element resource potential: an overview of metallogenetic provinces and their geodynamic setting. *Ore Geology Reviews*, **72**, 838–856.

Goryainov, S.V., Krylov, A.S., Vtyurin, A.N. and Pan, Y. (2015) Raman study of datolite CaBSiO$_4$(OH) at simultaneously high pressure and high temperature. *Journal of Raman Spectroscopy*, **46**, 177–181.

Haynes, C.V. (1965) Genesis of the White Cloud and related pegmatites, South Platte Area, Jefferson County, Colorado. *Geological Society of America Bulletin*, **76**, 441–462.

Holtstam, D. and Andersson U. (2007) The REE minerals of the Bastnäs-type deposits, south-central Sweden. *The Canadian Mineralogist*, **45**, 1073–1114.

Holtstam, D., Kolitsch, U. and Andersson, U.B. (2005) Västmanlandite-(Ce)-a new lanthanide-and F-bearing sorosilicate mineral from Västmanland, Sweden. *European Journal of Mineralogy*, **17**, 129–141.

Holtstam, D., Andersson, U.B., Broman C. and Mansfeld, J. (2014) Origin of REE mineralization in the Bastnäs-type Fe-REE-(Cu-Mo-Bi-Au) deposits, Bergslagen, Sweden. *Mineralium Deposita*, **49**, 933–966.

Jonsson, E. and Högdahl, K. (2013) New evidence for the timing of formation of Bastnäs-type REE mineralisation in Bergslagen, Sweden. *Mineral Deposit Research for a High-Tech World – Proceedings of the 12th Biennial SGA Meeting*, Uppsala, Sweden, 1724–1727.

Jonsson, E., Högdahl, K., Sahlström, F., Nysten, P. and Sadeghi, M. (2014) The Palaeoproterozoic skarn-hosted *REE* mineralisations of Bastnäs-type: overview and mineralogical-geological character. *ERES2014: 1st European Rare Earth Resources Conference, Milos – Book of abstracts*, 382–390.

Kjellman, J., Černý, P. and Smeds, S.A. (1999) Diversified NYF pegmatite populations of the Swedish Proterozoic: Outline of a comparative study. *The Canadian Mineralogist*, **37**, 832–833.

Laugier, J. and Bochu, B. (2004) *LMPG Suite of Programs for the Interpretation of X-ray Experiments*. ENSP/Laboratoire des Matériaux et du Génie Physique, BP 46. 38042 Saint Martin d'Hères, France. URL: http://www.ccp14.ac.uk/tutorial/lmgp/ (Accessed: 05 January 2017).

Lenz, C., Nasdala, L., Talla, D., Hauzenberger, C., Seitz, R. and Kolitsch, U. (2015) Laser-induced REE^{3+} photoluminescence of selected accessory minerals – An "advantageous artefact" in Raman spectroscopy. *Chemical Geology*, **415**, 1–16.

Lyalina, L.M., Selivanova, E.A., Savchenko, Y.E., Zozulya, D.R. and Kadyrova, G.I. (2014) Minerals of the gadolinite-(Y)-hingganite-(Y) series in the alkali granite pegmatites of the Kola Peninsula. *Geology of Ore Deposits*, **56**, 675–684.

McDonough, W.F. and Sun, S.S. (1995) The composition of the Earth. *Chemical Geology*, **120**, 223–253.

Merlet, C. (1994) An accurate computer correction program for quantitative electron probe microanalysis. *Microchimica Acta*, **114/115**, 363–376.

Miyawaki, R., Nakai, I. and Nagashima, K. (1984) A refinement of the crystal structure of gadolinite. *American Mineralogist*, **69**, 948–953.

Miyawaki, R., Matsubara, S., Yokoyama, K. and Okamoto, A. (2007) Hingganite-(Ce) and hingganite-(Y) from Tahara, Hirukawa-mura, Gifu Prefecture, Japan: The description on a new mineral species of the Ce-analogue of hingganite-(Y) with a refinement of the crystal structure of hingganite-(Y). *Journal of Mineralogical and Petrological Sciences*, **102**, 1–7.

Nasdala, L., Beyssac, O., Schopf, J.W. and Bleisteiner B. (2012) Application of Raman-based images in the Earth sciences. Pp. 145–187 in: *Raman Imaging – Techniques and Applications* (A. Zoubrir, editor). Springer Series Opti, **168**. Springer, Berlin -Heidelberg.

Nilssen, B. (1973) Gadolinite from Hundholmen, Tysfjord, North Norway. *Norsk Geologisk-Tidsskrift*, **53**, 343–348.

Pekov, I.V., Pasero, M., Yaskovskaya, A.N., Chukanov, N. V., Pushcharovsky, D.Y., Merlino, S., Zubkova, N.V., Kononkova, N.N., Menshikov, Y.P. and Zadov, A.E. (2007) Fluorcalciobritholite, $(Ca,REE)_5 [(Si,P)O_4]_3F$, a new mineral: description and crystal chemistry. *European Journal of Mineralogy*, **19**, 95–103.

Petříček, V., Dušek, M. and Palatinus, L. (2014) Crystallographic computing system JANA2006: general features. *Zeitschrift für Kristallographie*, **229**, 345–352.

Pezzotta, F., Diella, V. and Guastoni, A. (1999) Chemical and paragenetic data on gadolinite-group minerals from Baveno and Cuasso al Monte, southern Alps, Italy. *American Mineralogist*, **84**, 782–789.

Pieczka, A., Hawthorne, F.C., Cooper, M.A., Szełęg, E., Szuszkiewicz, A., Turniak, K., Nejbert, K. and Ilnicki, S. (2015) Pilawite-(Y), $Ca_2(Y, Yb)_2[Al_4(SiO_4)_4O_2 (OH)_2]$, a new mineral from the Piława Górna granitic pegmatite, southwestern Poland: mineralogical data, crystal structure and association. *Mineralogical Magazine*, **79**, 1143–1157.

Pršek, J., Ondrejka, M., Bačík, P., Budzyń, B. and Uher, P. (2010) Metamorphic-hydrothermal REE minerals in the Bacúch magnetite deposit, Western Carpathians, Slovakia: (Sr, S)-rich monazite-(Ce) and Nd-dominant hingganite. *The Canadian Mineralogist*, **48**, 81–94.

Sahlström, F., Jonsson, E., Högdahl, K., Harris, C., Troll, V.R. and Jolis, E.M. (2015) O and C isotope study of Bastnäs-type rare earth element mineralisation, Bergslagen, Sweden. *PacRim 2015 conference – Book of abstracts*, 439–443.

Segalstad, T.V. and Larsen, A.O. (1978) Gadolinite-(Ce) from Skien, southern Oslo region, Norway. *American Mineralogist*, **63**, 188–195.

Škoda, R., Cempírek, J., Filip, J., Novák, M., Veselovský, F. and Čtvrtlík, R. (2012) Allanite-(Nd), $CaNdAl_2Fe^{2+} (SiO_4)(Si_2O_7)O(OH)$, a new mineral from Åskagen, Sweden. *American Mineralogist*, **97**, 983–988.

Škoda, R., Plášil, J., Jonsson, E., Čopjaková, R., Langhof, J. and Vašinová Galiová, M. (2015) Redefinition of thalénite-(Y) and discreditation of fluorthalénite-(Y): A re-investigation of type material from the Österby pegmatite, Dalarna, Sweden, and from additional localities. *Mineralogical Magazine*, **79**, 965–984.

Smeds, S.A. (1990) Regional trends in mineral assemblages of Swedish Proterozoic granitic pegmatites and their geological significance. *Geologiska Föreningens i Stockholm Förhandlingar*, **112**, 227–242.

Vorma, A., Ojanperä, P., Hoffren, V., Siivola, J. and Löfgren, A. (1966) On the rare earth minerals from the Pyörönmaa pegmatite in Kangasala. *Comptes Rendu de la Société Geologique de Finlande*, **38**, 241–274.